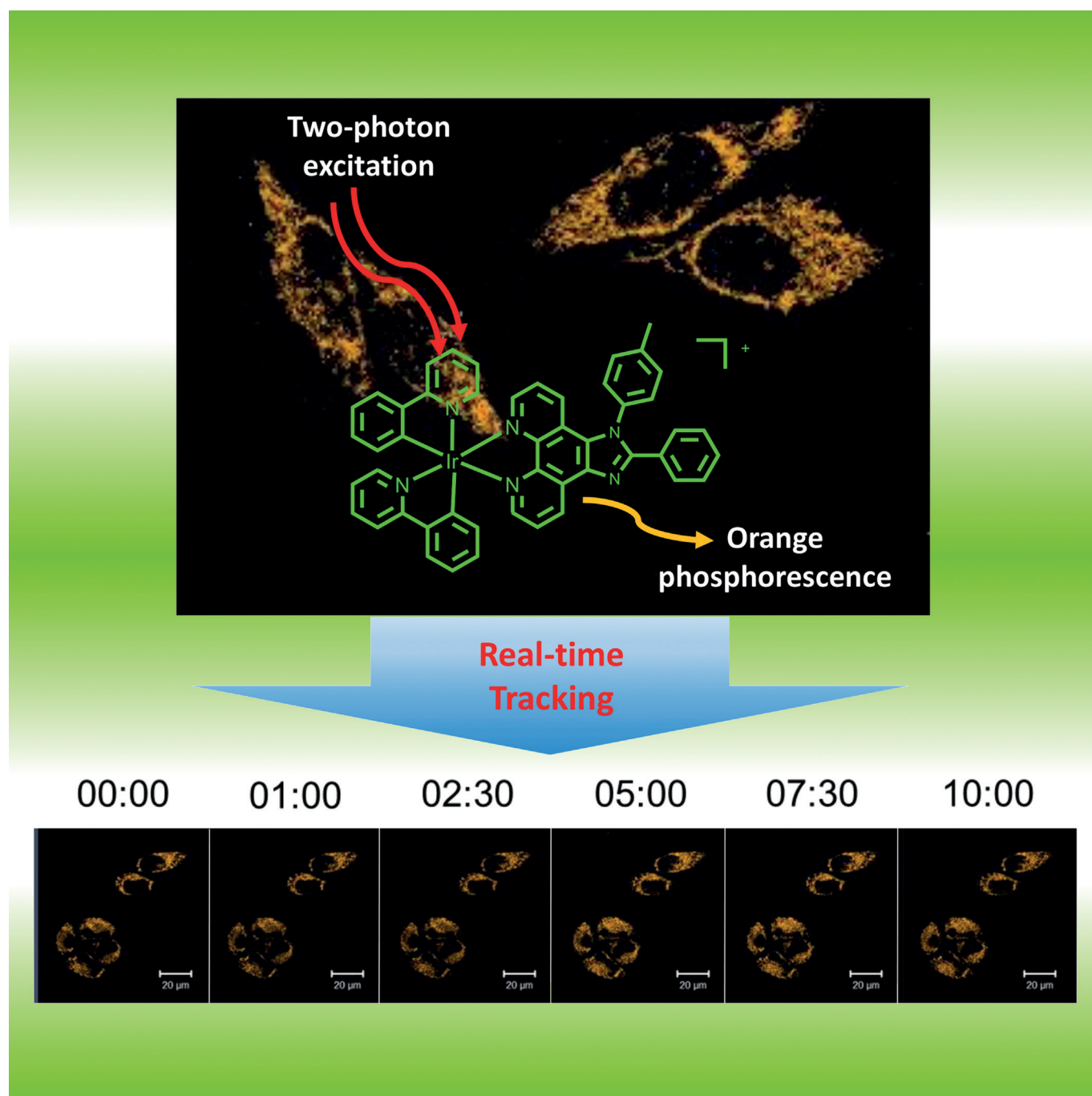


■ Imaging Agents

Cyclometalated Iridium(III) Complexes as Two-Photon Phosphorescent Probes for Specific Mitochondrial Dynamics Tracking in Living Cells

Chengzhi Jin, Jiangping Liu, Yu Chen, Leli Zeng, Ruilin Guan, Cheng Ouyang, Liangnian Ji, and Hui Chao^{*[a]}



Abstract: Five cyclometalated iridium(III) complexes with 2-phenylimidazo[4,5-*f*][1,10]phenanthroline derivatives (**IrL1–IrL5**) were synthesized and developed to image and track mitochondria in living cells under two-photon (750 nm) excitation, with two-photon absorption cross-sections of 48.8–65.5 GM at 750 nm. Confocal microscopy and inductive coupled plasma-mass spectrometry (ICP-MS) demonstrated that these complexes selectively accumulate in mitochondria within 5 min, without needing additional reagents for membrane permeabilization, or replacement of the culture

medium. In addition, photobleaching experiments and luminescence measurements confirmed the photostability of these complexes under continuous laser irradiation and physiological pH resistance. Moreover, results using 3D multicellular spheroids demonstrate the proficiency of these two-photon luminescent complexes in deep penetration imaging. Two-photon excitation using such novel complexes of iridium(III) for exclusive visualization of mitochondria in living cells may substantially enhance practical applications of bioimaging and tracking.

Introduction

Mitochondria, a membrane-bound organelle found in most eukaryotic cells, play a vital role in a variety of cellular processes, such as energy production, apoptosis regulation, central metabolism, calcium modulation and redox signaling.^[1] In addition, defects in mitochondrial function are directly related to aging, cancer, and neurodegenerative disorders including Alzheimer's, Huntington's, and Parkinson's diseases.^[2] These physiological and pathological processes involve subcellular level mitochondrial dynamics, including microtubule-based mitochondrial motility, mitochondrial fusion and fission and mitophagy-induced mitochondrial clearance.^[3] Designing probes to image and track mitochondria is crucial for linking changes in cell morphology to cellular functions.^[4] In luminescence bioimaging, luminescent probes are used to label specific biomolecules or subcellular organelles.^[5] To obtain high-resolution images at the subcellular level, organic organelle probes have been synthesized and commercialized, such as 4,6-diamidino-2-phenylindole (DAPI), rhodamine 123 and MitoTracker Green.^[6] However, most of the commercially available dyes suffer from notable shortcomings, including low water solubility, high toxicity to living cells, small Stokes shifts and poor photostability.^[7] These organic dyes may also cause extensive cellular damage and unwanted background signals due to the ultraviolet radiation required for their excitation.^[8] In addition, conventional organic dyes can be easily washed out when stained cells lose their mitochondrial potential, limiting their application for observing mitochondrial dynamics.^[9]

Compared to organic dyes, metal-based emissive dyes are interesting alternatives because they display many superior physicochemical properties for bioimaging, such as large Stokes shifts (hundreds of nm), long luminescence lifetimes (100 ns to 1 ms), and enhanced photostabilities (lower photobleaching).^[10] Although research on phosphorescent cyclometalated cationic Ir^{III} complexes as labels and sensors began late compared to research on the other transition metal complexes,^[11] they have been shown to have excellent photostability, good permeability of cell membranes and favorable quantum efficiency, which makes them attractive alternatives to fluorescent organic dyes for bioimaging and labelling.^[9,12] However, regrettably, for many Ir^{III} complexes, their one-photon absorbing (OPA) wavelength often lies in the bioincompatible ultraviolet region.^[13] Compared to OPA, excitation with the two-photon absorbing (TPA) wavelength in the near-infrared region has several advantages, including a high confined excitation capacity and intrinsic three-dimension resolution, as well as the ability to image at greater tissue depth, with reduced photodamage and background fluorescence.^[14] The 3D multicellular spheroid model is an alternative approach to analysis in living animals. This model provides a convenient way to adequately reflect the microenvironment of cells *in vivo* and better mimics the complex environment of animal tissue than do other models.^[15] The penetration depth of two-photon luminescence can be easily tested in this model due to its increased depth relative to a cell monolayer.

In previous research, we found that some Ir^{III} complexes possess high specificity for mitochondria and superior photostability, and can be used for mitochondrial imaging and tracking.^[9,12c,16] More importantly, Ir^{III} complexes have been developed as two-photon mitochondrial probes.^[16d,e] In the present work, to obtain specific novel complexes for mitochondrial two-photon phosphorescent probes, a series of 2-phenylimidazo-[4,5-*f*][1,10]phenanthroline derivatives that exhibited excellent light-emitting efficiency were synthesized and conjugated to iridium(III). The cellular location of these Ir^{III} complexes was determined using one-photon microscopy (OPM) and two-photon microscopy (TPM) imaging with MitoTracker Green FM (MTG) co-staining and inductively coupled plasma mass spectrometry (ICP-MS). We investigated the cytotoxicity and cellular uptake mechanism of all five Ir^{III} complexes (**IrL1–IrL5**), as well as the phosphorescence stability of **IrL1–IrL5** under photobleaching and pH fluctuation. Finally, using the 3D multicellular spheroid approach, we tracked and observed mitochondrial morphology at increasing imaging depths.

In previous research, we found that some Ir^{III} complexes possess high specificity for mitochondria and superior photostability, and can be used for mitochondrial imaging and tracking.^[9,12c,16] More importantly, Ir^{III} complexes have been developed as two-photon mitochondrial probes.^[16d,e] In the present work, to obtain specific novel complexes for mitochondrial two-photon phosphorescent probes, a series of 2-phenylimidazo-[4,5-*f*][1,10]phenanthroline derivatives that exhibited excellent light-emitting efficiency were synthesized and conjugated to iridium(III). The cellular location of these Ir^{III} complexes was determined using one-photon microscopy (OPM) and two-photon microscopy (TPM) imaging with MitoTracker Green FM (MTG) co-staining and inductively coupled plasma mass spectrometry (ICP-MS). We investigated the cytotoxicity and cellular uptake mechanism of all five Ir^{III} complexes (**IrL1–IrL5**), as well as the phosphorescence stability of **IrL1–IrL5** under photobleaching and pH fluctuation. Finally, using the 3D multicellular spheroid approach, we tracked and observed mitochondrial morphology at increasing imaging depths.

[a] C. Jin, J. Liu, Dr. Y. Chen, L. Zeng, R. Guan, C. Ouyang, Prof. L. Ji, Prof. Dr. H. Chao
MOE Key Laboratory of Bioinorganic and Synthetic Chemistry
School of Chemistry and Chemical Engineering, Sun Yat-Sen University
Guangzhou 510275 (P. R. China)
E-mail: ceschh@mail.sysu.edu.cn

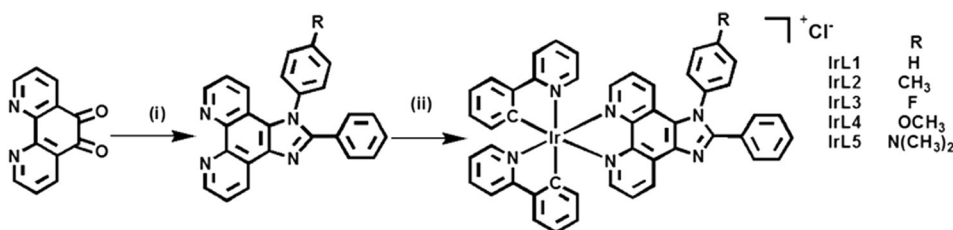
Supporting information for this article is available on the WWW under <http://dx.doi.org/10.1002/chem.201501882>.

Results and Discussion

Synthesis and characterization

A series of 2-phenylimidazo[4,5-*f*][1,10]phenanthroline derivatives (dpip = 1,2-diphenyl-1*H*-imidazo[4,5-*f*][1,10]phenanthroline; ptip = 2-phenyl-1-*p*-tolyl-1*H*-imidazo[4,5-*f*][1,10]phenanthroline; fpip = 1-(4-fluorophenyl)-2-phenyl-1*H*-imidazo[4,5-*f*][1,10]phenanthroline; mopip = 1-(4-methoxyphenyl)-2-phenyl-1*H*-imidazo[4,5-*f*][1,10]phenanthroline; and dmpip = *N,N*-dimethyl-4-(2-phenyl-1*H*-imidazo[4,5-*f*][1,10]phenanthrolin-1-yl)benzenamine) were synthesized using a “one-pot” method by mixing benzaldehyde, 1,10-phenanthroline-5,6-dione and substituted-aniline in acetic acid/NH₄Cl^[16b,17] as the chosen ligand. We prepared five Ir^{III} complexes by mixing [Ir(ppy)₂Cl]₂ and the corresponding ligands in aqueous CHCl₃/CH₃OH (2:1) and refluxing for 12 h (Scheme 1). All Ir^{III} complexes were purified by column chromatography and characterized by ES-MS, ¹H and ¹³C NMR spectroscopy (Figures S1–S10 in the Supporting Information).

Single crystals of the [Ir(ppy)₂ptip]Cl complexes (IrL2) and [Ir(ppy)₂dmpip]Cl (IrL5) were obtained by slowly evaporating the solvent at room temperature.



Scheme 1. Synthesis of IrL1–IrL5: i) formaldehyde, *p*-substituted aniline, NH₄Cl, acetic acid, 135 °C, 14 h; ii) [Ir(ppy)₂Cl]₂, CHCl₃/CH₃OH (v/v, 2:1), 65 °C, 12 h.

The crystal data and structural refinements are shown in Table 1. Selected bond lengths and angles are listed in Table 2.

The IrL2 and IrL5 complexes both crystallized in the *P* $\bar{1}$ triclinic space group. Ir1 iridium atoms within IrL2 had octahedral distortions, with the largest deviation observed in the bite angle (76.88°) of the ptip ligand (Figure 1). The bite angles of the IrL5 ligand (77.16°) were slightly larger than that of the ptip ligand. The lengths of the Ir–N bond in the cyclometalated ligands were 2.042 and 2.043 Å, respectively, which is shorter than that in the main ligand (2.144 and 2.157 Å). A similar observation was made for the IrL5 complex. The Ir–N distances in both IrL2 and IrL5 complexes are longer than those for ancillary ppy ligands, possibly due to a high *trans* influence.

This result is congruent with those observed for [Ir(ppy)₂-(PhenSe)]⁺.^[9] In the two Ir^{III} complexes, the main ligands ptip and dmpip have a tendency to form a large planar aromatic area and have the potential for larger two-photon absorption cross-sections.

Table 1. Crystal data and structure refinement for IrL2 and IrL5.

Identification code	IrL2	IrL5
empirical formula	C ₅₀ H ₃₆ Cl ₇ IrN ₆	C ₄₉ H ₃₈ ClIrN ₇
formula weight	1161.20	952.51
<i>T</i> [K]	150.0	153(2)
crystal system	triclinic	triclinic
space group	<i>P</i> $\bar{1}$	<i>P</i> $\bar{1}$
<i>a</i> [Å]	11.1667(4)	14.7899(6)
<i>b</i> [Å]	11.6133(4)	15.3662(7)
<i>c</i> [Å]	19.1520(6)	16.2713(9)
α [°]	107.603(3)	96.332(2)
β [°]	91.508(3)	116.5670(10)
γ [°]	101.386(3)	113.0000(10)
<i>V</i> [Å ³]	2310.93(14)	2856.2(2)
<i>Z</i>	2	2
ρ_{calcd} [g cm ⁻³]	1.669	1.108
μ [mm ⁻¹]	9.662	2.416
<i>F</i> (000)	1148.0	950.0
crystal size [mm ³]	0.38 × 0.35 × 0.14	0.143 × 0.119 × 0.105
radiation	CuK α (λ = 1.54178 Å)	MoK α (λ = 0.71073 Å)
2 θ range for data collection [°]	8.098 to 133.752	6.022 to 54.894
independent reflections	8069 [<i>R</i> _{int} = 0.0490, <i>R</i> _{sigma} = 0.0540]	12 603 [<i>R</i> _{int} = 0.0642, <i>R</i> _{sigma} = 0.0906]
data/restraints/parameters	8069/22/597	12603/67/511
GoF on <i>F</i> ²	1.065	1.015
final <i>R</i> indexes [<i>I</i> > 2 σ (<i>I</i>)]	<i>R</i> ₁ = 0.0421, <i>wR</i> ₂ = 0.1055	<i>R</i> ₁ = 0.0492, <i>wR</i> ₂ = 0.1142
final <i>R</i> indexes [all data]	<i>R</i> ₁ = 0.0468, <i>wR</i> ₂ = 0.1104	<i>R</i> ₁ = 0.0810, <i>wR</i> ₂ = 0.1323

Absorption and emission spectroscopy

The absorption and emission spectra of IrL1–IrL5 at 298 K in PBS buffer are shown in Figures S11 and S12, respectively, in the Supporting Information. The photophysical data are summarized in Table S1 in the Supporting Information. These complexes displayed weak absorp-

tion bands in the region of 330–400 nm, and stronger absorption bands in the region of 250–325 nm, which can be assigned to mixed singlet and triplet metal-to-ligand charge-transfers (¹MLCT and ³MLCT) and intraligand transitions (C–N ligands).^[18] The emission spectra of IrL1–IrL5 exhibit maximum peaks of approximately 595 nm with quantum yields (Φ) of 0.101–0.127, using [Ru(bpy)₃]²⁺ as a standard (Table S1 in the Supporting Information).^[19] Also, the effect of oxygen on the iridium luminescence was investigated. The results show that the quantum yields approximately doubled in degassed MeOH for all five complexes (Table S1 in the Supporting Information).^[20] The Stokes shifts of these values were approximately 210 nm. These large Stokes shifts offer advantages over commercial organic cellular dyes, such as rhodamine 6G and BIDOPY FL (Stokes shift = 30 and 8 nm, respectively).^[6]

Table 2. Select bond lengths and angles for IrL2 and IrL5.			
IrL2		IrL5	
bond lengths [Å]			
Ir1–N1	2.042(4)	Ir1–N1	2.045(6)
Ir1–N2	2.043(4)	Ir1–N2	2.010(5)
Ir1–N3	2.147(4)	Ir1–N3	2.150(4)
Ir1–N4	2.157(4)	Ir1–N4	2.140(4)
Ir1–C1	2.018(6)	Ir1–C1	2.018(6)
Ir1–C22	2.003(5)	Ir1–C12	1.997(6)
bond angles [°]			
N1–Ir1–N2	171.23(16)	N1–Ir1–N3	174.7(2)
N1–Ir1–N3	88.84(15)	N1–Ir1–N4	98.33(18)
N1–Ir1–N4	99.20(16)	N2–Ir1–N1	87.8(2)
N2–Ir1–N3	98.21(16)	N2–Ir1–N3	96.77(19)
N2–Ir1–N4	87.54(16)	N2–Ir1–N4	173.60(19)
N3–Ir1–N4	76.88(14)	N2–Ir1–C1	93.1(2)
C1–Ir1–N1	80.3(2)	N4–Ir1–N3	77.16(16)
C1–Ir1–N2	93.51(19)	C1–Ir1–N1	79.7(3)
C1–Ir1–N3	97.66(16)	C1–Ir1–N3	97.42(18)
C1–Ir1–N4	174.54(15)	C1–Ir1–N4	89.73(18)
C22–Ir1–N1	93.2(2)	C12–Ir1–N1	96.4(3)
C22–Ir1–N2	80.3(2)	C12–Ir1–N2	80.7(2)
C22–Ir1–N3	174.14(18)	C12–Ir1–N3	86.9(2)
C22–Ir1–N4	97.36(18)	C12–Ir1–N4	96.83(18)
C22–Ir1–C1	88.10(19)	C12–Ir1–C1	172.82(16)

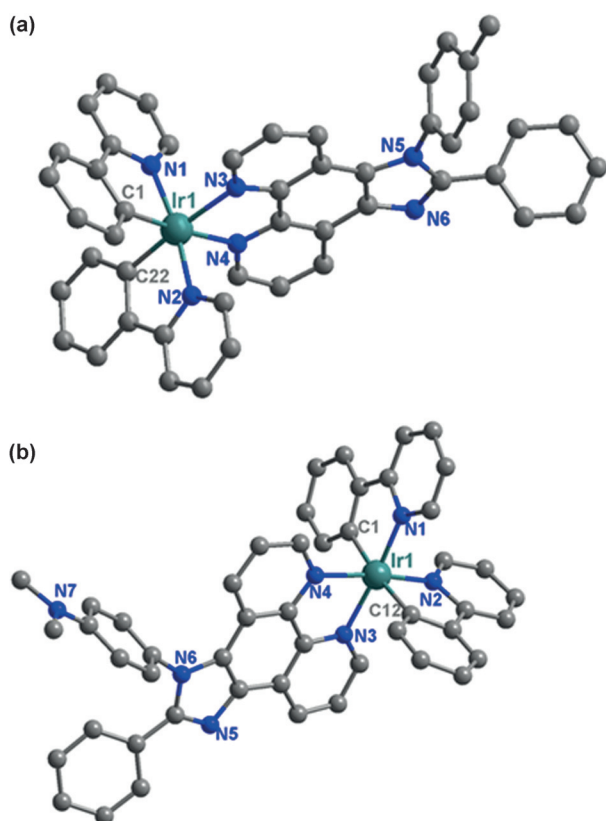


Figure 1. The structures of complexes: a) IrL2, and b) IrL5. For clarity, the solvent molecules, hydrogen atoms, and counterions are omitted.

Cytotoxicity measurements

An ideal cellular probe for practical application should minimally perturb living systems at the employed concentra-

tions.^[21] The cytotoxicity of the IrL1–IrL5 complexes was determined using an MTT assay after incubating HeLa cells with IrL1–IrL5.^[22] The time-dependent effects of IrL1–IrL5 on cell viability at 37 °C are shown in Figure 2. More than 90% of the cells survived after incubation with these agents for 12 h. These results suggest that all five Ir^{III} complexes exhibit low toxicities when imaging cells under the applied conditions (200 nM of complex incubated for 5 min).

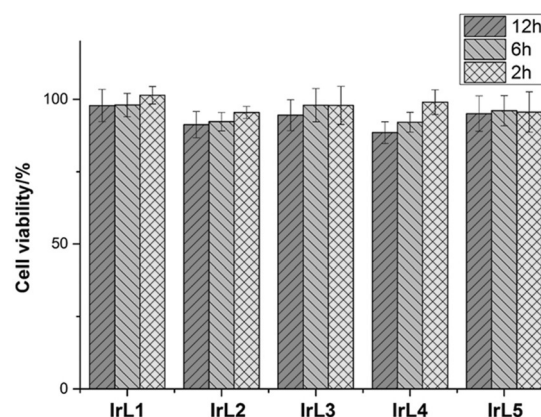


Figure 2. Viability of HeLa cells incubated with 0.2 μM IrL1–IrL5.

Cellular uptake and localization

To demonstrate that the specific localization of IrL1–IrL5 is in the mitochondria, co-localization imaging experiments were performed with these complexes using the commercially available mitochondrial dye, MitoTracker Green (MTG), to co-stain the HeLa cells. Because some complexes, such as [Ru(dip)₂-(dppz)]²⁺, can experience luminescence quenching in the presence of serum, we removed the serum before adding our Ir^{III} complexes.^[23] Interestingly, none of the studied complexes exhibited a significant difference when HeLa cells were incubated in media with or without fetal bovine serum (FBS). Incubation of 200 nM of IrL1–IrL5 in DMEM with 10% FBS for 5 min was followed by the removal of excess complex by washing with PBS three times and incubation using 50 nM MTG for 30 min. As shown in Figure 3, under these conditions, we observed excellent concordance between overlay images of the complexes and MTG, which suggested that IrL1–IrL5 is selectively localized within mitochondria. Pearson's co-localization coefficients,^[24] which measure the correlation of the intensity distribution between the Ir^{III} complexes and MTG signal, were 0.90, 0.92, 0.87, 0.85 and 0.86 for IrL1–IrL5, respectively. Because iridium is not an endogenous component of cells, accurate cellular uptake levels of Ir^{III} can be determined quantitatively using ICP-MS.^[25] We performed ICP-MS experiments for each IrL1–IrL5 complex at a staining concentration of 200 nM. The ICP-MS measurements (Figure S13 in the Supporting Information) indicated that very high levels of IrL1–IrL5 accumulated in mitochondria. For all five Ir^{III} complexes, the ratios of mitochondrial Ir-to-whole cell Ir (nuclei + cytoplasm) were more than 80%, and the ratios for IrL1 and IrL2 surpassed 90% (91.3 and 91.1%, respectively). To rationally determine our incubation

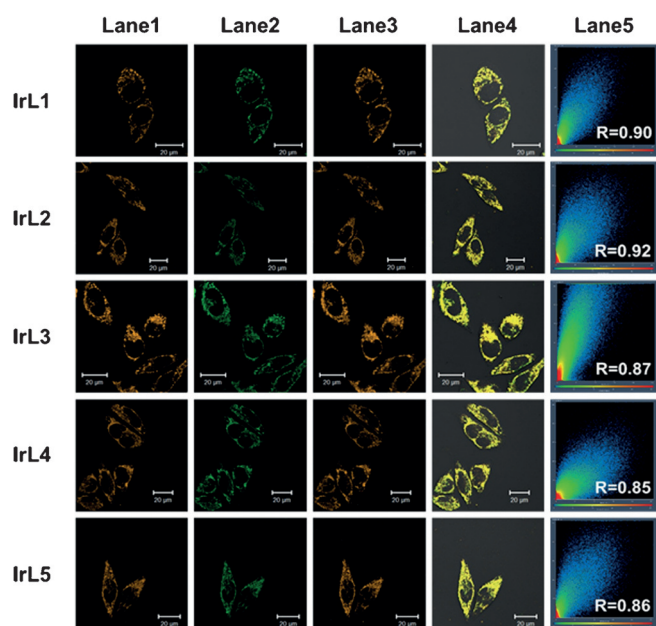


Figure 3. OPM and TPM confocal phosphorescence images and their overlays with bright-field images of living HeLa cells incubated with 200 nm of IrL1–IrL5 in DMSO and DMEM with 10% FBS (pH 7.4, 1:999, v/v) for 5 min at 37 °C followed by 50 nm of MTR. Lane 1: OPM confocal phosphorescence images of IrL1–IrL5; lane 2: confocal phosphorescence images of MTG; lane 3: TPM confocal phosphorescence images of IrL1–IrL5; lane 4: overlay of lane 1, lane 2, lane 3 and bright field; lane 5: the overlap coefficient of columns lane 1 and lane 2, and Pearson's co-localization coefficients are also presented. Excitation wavelength: 405 nm (OPM for all Ir^{III} complexes), 750 nm (TPM for all Ir^{III} complexes), 488 nm (for MTG); emission filter: 595(±30) nm (for all Ir^{III} complexes) and 520(±20) nm (for MTG). Scale bars: 20 μm.

time, time-dependent cellular uptake of IrL2 using real-time imaging and ICP-MS were conducted, and the results (Figures S14 and S15 in the Supporting Information) demonstrate that uptake of Ir^{III} complexes reached saturation within 6 min. The imaging results revealed that at a low concentration (200 nm), all of these complexes quickly crossed the membrane (within 5 min) and selectively accumulated in mitochondria (above 80%, IrL1 and IrL2 above 90%).

Mechanisms of cellular uptake

Cellular uptake of small molecules can occur through energy-independent (diffusion, passive diffusion) and energy-dependent (endocytosis, active transport) pathways.^[26] To explore the mechanism of cellular entry, we selected IrL2 as an example to investigate its cellular uptake at varying temperatures and different metabolic and endocytic levels.

Blockage of cellular uptake was observed using confocal luminescence microscopy when the cell was incubated at 4 °C or pretreated with metabolic inhibitors (2-deoxy-D-glucose and oligomycin).^[23,27] As shown in Figure 4a and d, the intracellular luminescence was too weak to be visualized. In addition, when the incubation temperature was set to 20 °C (Figure 4b), the intracellular luminescence was recovered but remained weaker than luminescence at 37 °C (Figure 4c). Based on this observation, energy seems to play a significant role in the IrL2 com-

plex crossing the plasma membrane to localize in mitochondria; the activity of several proteins that aid membrane crossing may be inhibited when the incubation temperature is less than 37 °C. As a general cell entry mechanism that involves receptor signaling (including signaling from receptor tyrosine kinases and G protein-coupled receptors), endocytic membrane trafficking is energy-dependent.^[28] Thus, inhibitors of endocytosis (chloroquine and NH₄Cl) were used to investigate IrL2 entry into cells.^[29] The confocal image revealed that endocytosis inhibition does not block IrL2 from crossing the membrane (Figure 4e and f). In addition, these results were confirmed by flow cytometry (Figure S16 in the Supporting Information). Furthermore, entry by the endocytotic pathway is typically a slow process.^[37,38] Time-dependent ICP-MS results indicated that IrL2 uptake reached a maximum within 5 min (Figure S14 in the Supporting Information). These results suggest that the endocytotic pathway is not responsible for the mitochondrial localization of IrL2. In summary, IrL2 crosses the plasma membrane using non-endocytic energy-dependent active transport. Considering the structural similarity of these five Ir^{III} complexes, the other complexes may share similar mechanisms of transmembrane transport.

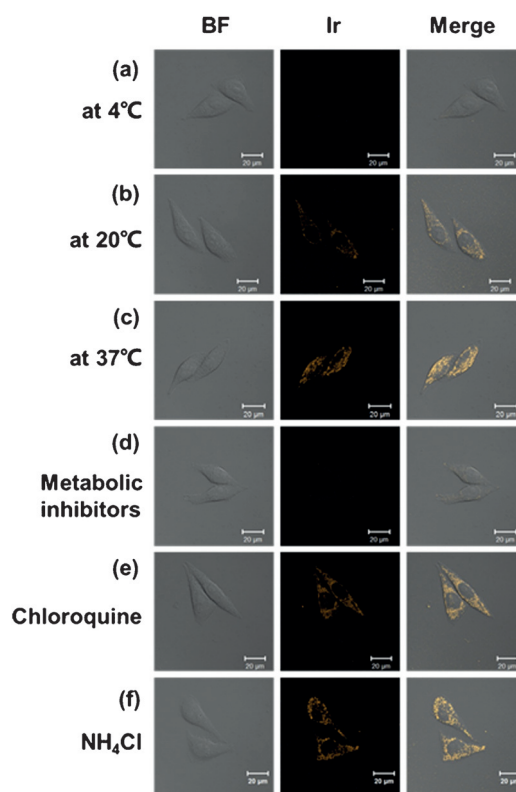


Figure 4. Confocal luminescence image and bright-field images of living HeLa cells incubated with 200 nm IrL2 in DMSO/PBS (pH 7.4, 1:999, v/v) under different conditions. a) Cells incubated with 200 nm IrL2 at 4 °C for 5 min; scale bars: 100 μm. b) Cells incubated with 200 nm Mitolr7 at 20 °C for 5 min. c) Cells incubated with 200 nm IrL2 at 37 °C for 5 min. d) Cells pre-incubated with 50 mM 2-deoxy-D-glucose and 5 μM oligomycin in PBS for 1 h at 37 °C and then incubated with 200 nm IrL2 at 37 °C for 5 min. e, f) Cells pretreated with endocytic inhibitors (chloroquine (50 μM) and NH₄Cl (50 mM), respectively) and then incubated with 200 nm IrL2 at 37 °C for 15 min (λ_{ex} = 405 nm, λ_{em} = 595(±30) nm). Scale bars: 20 μm.

Two-photon absorption (TPA) cross-sections

The phosphorescence quantum yields of the five complexes were 0.108–0.127. The TPA cross-sections of these complexes were determined at the wavelength range of 720–860 nm in CH₃OH (500 mM). From the log–log plot of the emission intensity against incident power, the linear regression slopes of 1.85 ± 0.05 , 2.04 ± 0.06 , 2.07 ± 0.07 , 2.04 ± 0.07 and 2.05 ± 0.04 , respectively, indicate a two-photon excitation process (Figures S17–S21 in the Supporting Information). The two-photon absorption cross-section of the complexes were measured as 61.7, 65.5, 48.8, 49.7 and 52.0 GM (1 GM = $10 \times 50 \text{ cm}^4 \text{ s photon}^{-1}$), using rhodamine B as the standard (Figure 5).^[30] As suggested by Furuta et al., TPA cross-section values should be higher than 0.1 GM for optical imaging applications in live specimens. The values of our complexes not only meet the requirements mentioned above but also exceed those of some reported for mononuclear transition metal complexes.^[31]

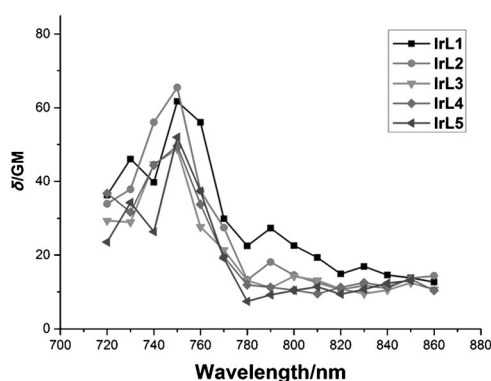


Figure 5. Two-photon absorption cross-section of IrL1–IrL5 at different excitation wavelength. The maximum TPA cross-sections value is 65.5 GM (IrL2) at 750 nm.

One- and two-photon imaging of Ir^{III} complexes in 3D multicellular spheroids

There remain significant technical challenges to increasing the imaging depth for microscopic study of living tumor spheroids. 3D multicellular spheroids contain an extensive extracellular matrix (ECM) that differ in their relative amounts and in their assembly in corresponding monolayer cultures.^[32] Thus, in this work, 3D multicellular spheroids were imaged under confocal laser scanning microscopy to demonstrate the 3D distribution and two-photon penetration of Ir^{III} complexes. For IrL2, after treatment with Ir^{III} complexes, phosphorescence was observed from the surface of the spheroids to a depth of approximately 90 μm for one-photon excitation and about 250 μm for two-photon excitation. The phosphorescent images were captured every 6.9 μm along the Z-axis. The spheroids exhibited much stronger phosphorescence in deep layer cells using two-photon excitation than one-photon excitation, indicating deeper penetration of two-photon excitation light with an incubation of 30 min (Figure 6). The results of the incubation

demonstrated that the rising cell numbers and the presence of ECM that accompany the formation of 3D multicellular spheroids do not significantly impede the speed at which these Ir^{III} complexes cross the membrane. However, one noteworthy feature is that the inner core of the 3D multicellular spheroids cannot take in the Ir^{III} complexes even after extending the incubation time to 8 h and increasing the concentration to 2 μM (Figure S22 in the Supporting Information). This phenomenon may be attributed to the mechanism of uptake, which involves energy-dependent active transport; the necrotic cells in the core are unable to perform this process.^[33] Similar results were observed when the spheroids were pretreated with IrL1, IrL3, IrL4 and IrL5 (Figures S23–S26 in the Supporting Information). In summary, the penetrating depth we observed for these Ir^{III} complexes highlights their value in 3D observation using two-photon imaging.

Photobleaching and pH-dependent luminescent stability experiments

Photostability is one of the most important criteria for developing fluorescent imaging agents.^[34] The photostability of all five Ir^{III} complexes compared to those of the organic dyes under continuous laser irradiation was determined using time-dependent imaging of Ir^{III} complexes and MTG co-stained HeLa cells. The initial intensities from the first scans at a co-stained cell concentration of 5 μM were normalized before calculating decreases in percentage of fluorescence. As shown in Figure 7a, using IrL2 versus MTG as an example, during 20 scans with a total irradiation time of approximately 5 min, almost no significant luminescence was observed in the MTG image, whereas no obvious change in the luminescence was observed for IrL2. Statistically, as shown in Figure 7b, after 20 scans, the fluorescence signal intensity of MTG decreased to approximately 33%. In contrast, the signal intensity of the Ir^{III} complexes merely slightly declined. The photobleaching properties of IrL1–IrL5 (except IrL2) are listed in Figures S27–S30 in the Supporting Information. For biological applications, dyes should be usable within a particular pH range.^[17] Therefore, we investigated the effect of pH variation from 4 to 10 on the luminescence of the Ir^{III} complexes. The results indicate that the luminescence of all Ir^{III} complexes except IrL5 changed very little when the pH was in the physiological range. This result may be due to the blockage of the N atom in the imidazole group of their structures. A mild decrease in luminescence was observed for IrL5, which may be due to the presence of an $-\text{N}(\text{CH}_3)_2$ group (Figure S31 in the Supporting Information).

Tracking mitochondrial morphological changes

Mitochondria are the organelles in which cellular respiration occurs. Mitochondria continuously oxidize substrates and maintain a proton gradient across the lipid bilayer with a very large membrane potential of approximately 180 mV.^[35] Variation in the membrane potential of mitochondria in cells has evolved as a read-out of mitochondrial functional status and generates signals to activate pathways that repair or eliminate

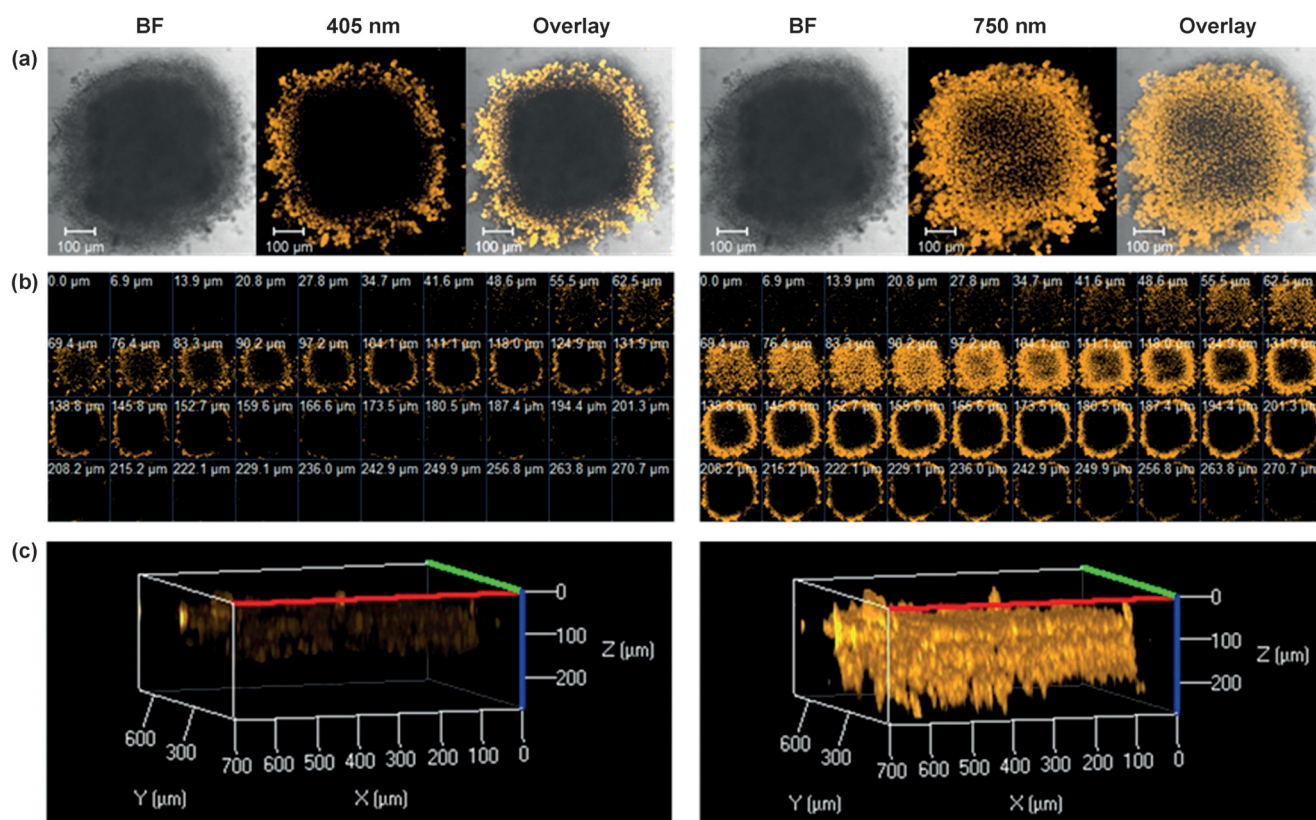


Figure 6. a) OPM (left) and TPM (right) images of 3D multicellular spheroids after incubation with IrL2 (500 nm) for 0.5 h. b) Z-stack images were taken every approximately 7 μm section along the Z-axis of an intact spheroid. c) The merged images of Z-stack images of an intact spheroid. The wavelengths for one- and two-photon excitation were set as 405 and 750 nm, respectively. The images were taken under 10 \times objective. Scale bars: 100 μm .

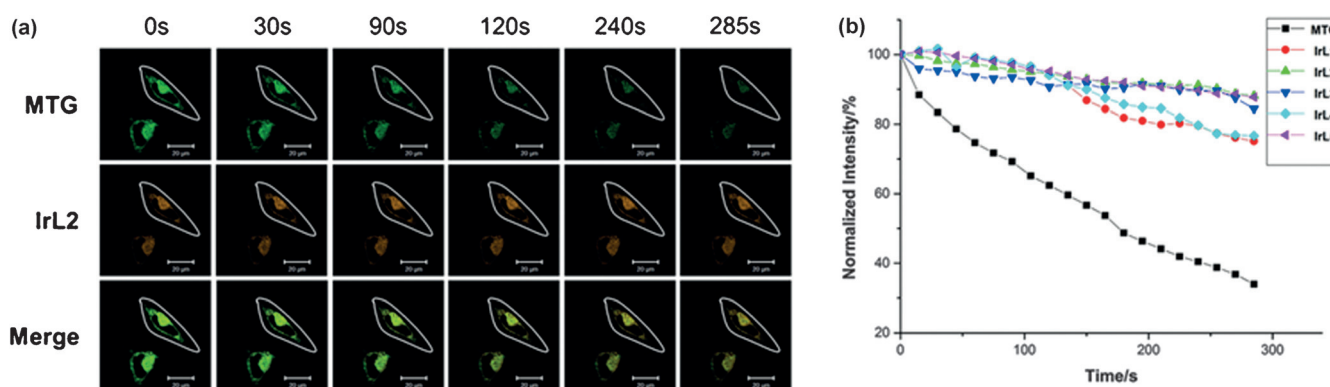


Figure 7. Photobleaching experiments of the Ir^{III} complexes in HeLa cells. a) Time-dependent confocal imaging of IrL2/MTG co-stained HeLa cells. Time interval: 15 s. Scale bar: 20 μm ($\lambda_{\text{ex}} = 405 \text{ nm}$, $\lambda_{\text{em}} = 595(\pm 30) \text{ nm}$). b) Quantitative photobleaching results indicate that IrL1–IrL5 exhibited robust emission intensity under continuous light irradiation.

defective mitochondria.^[36] Therefore, tracking the mitochondrial morphological changes related to a variety of cellular functions may provide insight into the conditions that are associated with apoptosis and degeneration.^[37] However, commercial organic dyes, such as MTG, will lose their specificity to mitochondria when cells are treated with the uncoupler 3-chlorophenylhydrazon (CCCP).^[38] In contrast, IrL1–IrL5 have a high tolerance to decreases in mitochondrial membrane potential. Using IrL2 as an example, reticulum-like mitochondria were

gradually transformed into small and dispersed fragments upon exposure to CCCP, as shown in Figure 8 (Video S1 in the Supporting Information), consistent with the morphological changes of mitochondria in the early stages of apoptosis. These processes are involved in the remodeling of mitochondrial cristae and the mobilization of cytochrome c, which is considered an irreversible process associated with the collapse of the membrane potential.^[39] Similar results were observed when we used IrL1, IrL3, IrL4 and IrL5 to conduct this experi-

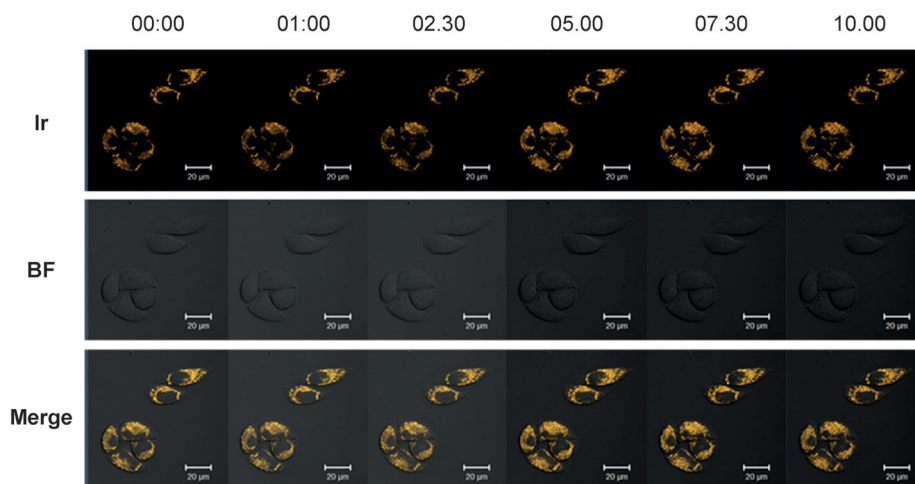


Figure 8. Phosphorescence images of CCCP (20 μM) treated living HeLa cells stained with IrL2 (200 nM) with increasing scan time (the scan time is shown in the upper panel). The upper panel is the luminescence images of IrL2. The middle panels are the bright-field images. The lower panels are the merged images. ($\lambda_{\text{ex}} = 405 \text{ nm}$, $\lambda_{\text{em}} = 595(\pm 30) \text{ nm}$).

ment (Figures S32–S35 in the Supporting Information), which is consistent with previous results from our laboratory with similar complexes.^[16c]

Conclusion

In conclusion, a new series of Ir^{III} complexes (IrL1–IrL5) with two-photon luminescence have been synthesized and utilized as agents for mitochondrial imaging and tracking in monolayer cells. The two-photon penetrating depth of the Ir^{III} complexes was evaluated using 3D multicellular spheroids. These complexes have numerous advantages for two-photon imaging, including rapid incubation time (5 min for monolayer cells and 30 min for 3D multicellular spheroids), appreciable photostability, excellent pH resistance, low imaging concentration (200 nM), low cytotoxicity at the imaging concentration, and sufficient TPA cross-sections for imaging. Cellular uptake experiments indicated that these Ir^{III} complexes cross the membrane using non-endocytosis active transport. Moreover, the Ir^{III} complexes have a high resistance to decreases in the mitochondrial membrane potential, making them suitable for tracking mitochondrial morphological changes during the early stages of apoptosis, which highlights their potential for applications in biomedical research.

Experimental Section

Characterization

¹H NMR spectra were recorded using a 300 MHz nuclear magnetic resonance spectrometer (Varian, Mercury-Plus 300) and Bruker 500 nuclear magnetic resonance spectrometer. All chemical shifts are reported relative to tetramethylsilane (TMS). The electronic absorption spectra were recorded using a Perkin–Elmer Lambda 850 UV/Vis spectrometer. The emission spectra were recorded using a Perkin–Elmer LS 55 luminescence spectrometer. Microanalysis (C, H, and N) was carried out using an Elementar Vario EL elemental

analyzer. Electrospray mass spectra were recorded using an LCQ system (Finnigan MAT).

Materials and synthesis

All reactants and solvents were purchased from commercial sources and used as received unless otherwise stated. All procedures involving IrCl₃·xH₂O were carried out under an argon atmosphere.

Synthesis of ligands and the corresponding iridium(III) complexes

1,10-Phenanthroline-5,6-dione^[40] and [Ir(ppy)₂Cl]₂^[41] were synthesized according to previously published methods.

1,2-Diphenyl-1H-imidazo[4,5-f]

[1,10]phenanthroline (dpip): A mixture of 1,10-phenanthroline-

5,6-dione (0.525 g, 2.5 mmol), ammonium acetate (3.85 g, 50 mmol), benzaldehyde (0.265 g, 2.5 mmol), aniline (0.233 g, 2.5 mmol) and glacial acetic acid (10 cm³) was refluxed under argon for 14 h. Then, the reaction mixture was cooled to room temperature and poured into water (30 cm³). The solution was neutralized with 25% NH₃ aqueous solution and extracted with dichloromethane (20 mL×3). The organic phase was dried over MgSO₄, and the solvent was removed under vacuum. The crude product was purified by column chromatography on silica with CH₂Cl₂/ethanol (20:1, v/v) as the eluent. The resulting solid was recrystallized from chloroform/toluene to afford a white microcrystal. Yield, 0.756 g, 81.3%; elemental analysis calcd (%) for C₂₅H₁₆N₄: C 80.63, H 4.33, N 15.04; found: C 80.54, H 4.65, N 15.11; ¹H NMR (300 MHz, [D₆]DMSO): $\delta = 9.07$ (dd, $J = 4.2, 1.8 \text{ Hz}$, 1H), 9.00 (dd, $J = 8.1, 1.8 \text{ Hz}$, 1H), 8.93 (dd, $J = 4.3, 1.6 \text{ Hz}$, 1H), 7.86 (dd, $J = 8.1, 4.2 \text{ Hz}$, 1H), 7.73 (ddd, $J = 15.6, 8.4, 4.5 \text{ Hz}$, 5H), 7.61–7.55 (m, 2H), 7.47 (dd, $J = 8.4, 4.2 \text{ Hz}$, 1H), 7.40–7.30 ppm (m, 4H); ES-MS (CH₂Cl₂): m/z 373.1 [M+H]⁺, 767.4 [2M+Na]⁺.

2-Phenyl-1-p-tolyl-1H-imidazo[4,5-f][1,10]phenanthroline (ptip):

This compound was synthesized in a manner identical to that described for ligand dpip but using *p*-toluidine (0.268 g, 2.5 mmol) instead of aniline. Yield: 0.737 g, 76.4%; elemental analysis calcd (%) for C₂₆H₁₈N₄: C 80.81, H 4.69, N 14.50; found: C 80.93, H 4.36, N 14.41; ¹H NMR (300 MHz, CDCl₃): $\delta = 9.24$ –9.10 (m, 2H), 9.03 (s, 1H), 7.75 (dd, $J = 8.1, 4.2 \text{ Hz}$, 1H), 7.66–7.52 (m, 4H), 7.44 (t, $J = 9.3 \text{ Hz}$, 3H), 7.35–7.26 (m, 4H), 1.45–1.43 ppm (m, 3H); ES-MS (CH₂Cl₂): m/z 387.1 [M+H]⁺, 795.4 [2M+Na]⁺.

1-(4-Fluorophenyl)-2-phenyl-1H-imidazo[4,5-f][1,10]phenanthroline (fpip):

This compound was synthesized in a manner identical to that described for ligand dpip but using 4-fluoroaniline (0.278 g, 2.5 mmol) instead of aniline. Yield: 0.801 g, 82.2%; elemental analysis calcd (%) for C₂₅H₁₅FN₄: C 72.60, H 3.87, N 14.35; found: C 72.67, H 4.03, N 14.22; ¹H NMR (300 MHz, DMSO): $\delta = 9.07$ (s, 1H), 9.03–8.85 (m, 2H), 7.84 (s, 3H), 7.62–7.45 (m, 5H), 7.39 ppm (s, 4H); ES-MS (CH₂Cl₂): m/z 391.1 [M+H]⁺, 803.3 [2M+Na]⁺.

1-(4-Methoxyphenyl)-2-phenyl-1H-imidazo[4,5-f][1,10]phenanthroline (mopip):

This compound was synthesized in a manner identical to that described for ligand dpip but using 4-methoxyaniline (0.308 g, 2.5 mmol) instead of aniline. Yield: 0.722 g, 71.2%; el-

emental analysis calcd (%) for $C_{26}H_{18}N_4O$: C 77.59, H 4.51, N 13.92; found: C 72.66, H 4.37, N 13.98; 1H NMR (300 MHz, DMSO): δ = 8.99 (dd, J = 22.2, 14.4 Hz, 3H), 7.84 (s, 1H), 7.74–7.55 (m, 4H), 7.51 (s, 1H), 7.41 (d, J = 14.1 Hz, 4H), 7.20 (d, J = 8.1 Hz, 2H), 3.88 ppm (s, 3H); ES-MS (CH_2Cl_2): m/z 403.1 $[M+H]^+$, 827.3 $[2M+Na]^+$.

***N,N*-Dimethyl-4-(2-phenyl-1*H*-imidazo[4,5-*f*][1,10]phenanthrolin-1-yl)benzenamine (dmpip)**: This compound was synthesized in a manner identical to that described for ligand dpip but using *N*1,*N*1-dimethylbenzene-1,4-diamine (0.341 g, 2.5 mmol) instead of aniline. Yield: 0.582 g, 56.1%; elemental analysis calcd (%) for $C_{27}H_{21}N_5$: C 78.05, H 5.09, N 16.86; found: C 78.11, H 5.25, N 16.77; 1H NMR (300 MHz, $CDCl_3$): δ = 9.20–9.07 (m, 2H), 9.03 (d, J = 4.2 Hz, 1H), 7.73 (dd, J = 8.3, 4.5 Hz, 1H), 7.64 (dd, J = 16.5, 6.3 Hz, 3H), 7.31 (dd, J = 10.2, 6.3 Hz, 6H), 6.82 (d, J = 8.6 Hz, 2H), 3.11 ppm (s, 6H); ES-MS (CH_2Cl_2): m/z 416.1 $[M+H]^+$, 853.3 $[2M+Na]^+$.

[Ir(ppy)₂dpip]Cl (IrL1): This complex was synthesized as described below. A chloro-bridged dimer $[Ir(ppy)_2Cl]_2$ (0.088 g, 0.08 mmol) and dpip (0.056 g, 0.015 mmol) were placed in a 100 mL round-bottom flask with 40 mL of methanol and CH_2Cl_2 (1:1, v/v). The mixture was heated at 65 °C for 12 h under argon. After the solution cooled to room temperature, the solvent was removed under vacuum to afford a bright yellow precipitate. The product was purified by column chromatography on alumina using acetonitrile/ethanol (20:1, v/v) as the eluent. Yield: 0.0971 g, 71.3%; elemental analysis calcd (%) for $C_{47}H_{32}N_6ClIr$: C 62.14, H 3.55, N 9.25; found: C 62.27, H 3.75, N 9.17; 1H NMR (500 MHz, $[D_6]DMSO$): δ = 9.31 (dd, J = 8.5, 1.4 Hz, 1H), 8.30–8.24 (m, 3H), 8.23 (d, J = 3.5 Hz, 1H), 8.14 (dd, J = 8.5, 5.0 Hz, 1H), 8.08 (d, J = 4.5 Hz, 1H), 7.94 (dd, J = 16.0, 8.0 Hz, 2H), 7.90–7.86 (m, 2H), 7.80–7.68 (m, 6H), 7.62 (d, J = 7.0 Hz, 2H), 7.53–7.38 (m, 7H), 7.09–6.99 (m, 4H), 6.97–6.91 (m, 2H), 6.28 ppm (dd, J = 16.0, 7.5 Hz, 2H); ^{13}C NMR (125 MHz, $[D_6]DMSO$): δ = 171.90, 167.32, 154.30, 150.99, 150.59, 149.74, 149.56, 148.77, 145.11, 144.74, 144.45, 139.22, 137.06, 136.55, 132.93, 131.66, 131.59, 131.27, 130.75, 130.49, 130.12, 129.75, 129.55, 129.29, 129.00, 128.24, 127.01, 126.52, 125.58, 124.37, 124.29, 122.86, 122.53, 120.52 ppm; ES-MS (CH_3OH): m/z 873.25 $[M-Cl]^-$.

[Ir(ppy)₂ptip]Cl (IrL2): This compound was synthesized in a manner identical to that described for $[Ir(ppy)_2pi]Cl$ but using ptip (0.058 g, 0.015 mmol) instead of dpip. Yield: 0.1036 g, 74.9%; elemental analysis calcd (%) for $C_{48}H_{34}N_6ClIr$: C 62.50, H 3.71, N 9.11; found: C 62.63, H 3.92, N 9.05; 1H NMR (500 MHz, $[D_6]DMSO$): δ = 9.30 (dd, J = 8.5, 1.5 Hz, 1H), 8.29–8.21 (m, 3H), 8.14 (dd, J = 8.5, 5.0 Hz, 1H), 8.08 (d, J = 5.0 Hz, 1H), 7.94 (dd, J = 15.0, 8.0 Hz, 2H), 7.88 (q, J = 7.5 Hz, 2H), 7.78 (dd, J = 8.5, 5.0 Hz, 1H), 7.64 (dd, J = 13.0, 5.5 Hz, 4H), 7.57–7.39 (m, 8H), 7.08–6.98 (m, 4H), 6.94 (dtd, J = 11.0, 7.5, 1.2 Hz, 2H), 6.27 (dd, J = 13.0, 7.5 Hz, 2H), 2.48 ppm (s, 3H); ^{13}C NMR (125 MHz, $[D_6]DMSO$): δ = 167.32, 154.42, 151.02, 150.59, 149.70, 149.59, 148.73, 145.08, 144.72, 144.45, 141.28, 139.22, 136.51, 134.44, 132.91, 131.67, 130.75, 130.45, 130.14, 129.75, 129.64, 129.01, 128.95, 128.25, 127.01, 126.53, 125.58, 124.38, 124.30, 122.88, 122.59, 120.52, 21.47 ppm; ES-MS (CH_3OH): m/z 887.25 $[M-Cl]^-$.

[Ir(ppy)₂fpip]Cl (IrL3): This compound was synthesized in a manner identical to that described for $[Ir(ppy)_2pi]Cl$ but using fpip (0.059 g, 0.015 mmol) instead of dpip. Yield: 0.0895 g, 64.4%; elemental analysis calcd (%) for $C_{47}H_{31}N_6FCIr$: C 60.93, H 3.37, N 9.07; found: C 60.88, H 3.56, N 9.13; 1H NMR (500 MHz, $[D_6]DMSO$): δ = 9.31 (dd, J = 8.5, 1.5 Hz, 1H), 8.29–8.22 (m, 3H), 8.14 (dd, J = 8.5, 5.0 Hz, 1H), 8.10 (d, J = 5.0 Hz, 1H), 7.98–7.85 (m, 6H), 7.81 (dd, J = 8.5, 5.0 Hz, 1H), 7.61 (d, J = 7.5 Hz, 4H), 7.52–7.42 (m, 5H), 7.09–6.92 (m, 6H), 6.28 ppm (dd, J = 15.0, 7.5 Hz, 2H); ^{13}C NMR (125 MHz, $[D_6]DMSO$): δ = 167.34, 162.41, 154.53, 150.99, 150.59,

149.78, 149.52, 148.87, 145.05, 144.71, 144.44, 139.23, 136.49, 133.33, 132.91, 131.67, 130.77, 130.52, 130.41, 129.83, 129.48, 129.05, 128.32, 128.27, 127.25, 126.48, 125.59, 124.37, 124.29, 122.89, 122.51, 120.54, 118.38, 118.20 ppm; ES-MS (CH_3OH): m/z 891.25 $[M-Cl]^-$.

[Ir(ppy)₂mopip]Cl (IrL4): This compound was synthesized in a manner identical to that described for $[Ir(ppy)_2pi]Cl$ but using mopip (0.049 g, 0.015 mmol) instead of dpip. Yield: 0.1086 g, 77.2%; elemental analysis calcd (%) for $C_{48}H_{34}N_6OClIr$: C 61.43, H 3.65, N 8.96; found: C 61.56, H 3.77, N 8.91; 1H NMR (500 MHz, $[D_6]DMSO$): δ = 9.30 (dd, J = 8.5, 1.5 Hz, 1H), 8.29–8.21 (m, 3H), 8.13 (dd, J = 8.5, 5.0 Hz, 1H), 8.08 (d, J = 5.0 Hz, 1H), 7.94 (dd, J = 14.0, 7.5 Hz, 2H), 7.88 (q, J = 7.5 Hz, 2H), 7.80 (dd, J = 8.5, 5.0 Hz, 1H), 7.69 (dd, J = 6.0, 3.0 Hz, 2H), 7.62 (dd, J = 21.0, 7.0 Hz, 3H), 7.50–7.42 (m, 5H), 7.26–7.18 (m, 2H), 6.98 (dddt, J = 15.0, 10.0, 7.5, 4.5 Hz, 6H), 6.28 (dd, J = 14.0, 7.5 Hz, 2H), 3.88 ppm (s, 3H); ^{13}C NMR (125 MHz, $[D_6]DMSO$): δ = 171.91, 167.33, 161.06, 154.57, 151.03, 150.62, 149.67, 149.54, 148.74, 145.06, 144.70, 144.45, 139.22, 136.41, 132.88, 131.66, 130.75, 130.44, 130.25, 129.73, 129.36, 129.02, 128.47, 128.21, 127.07, 126.52, 125.58, 124.37, 124.30, 122.87, 122.64, 120.52, 116.27, 56.16 ppm; ES-MS (CH_3OH): m/z 903.25 $[M-Cl]^-$.

[Ir(ppy)₂dmpip]Cl (IrL5): This compound was synthesized in a manner identical to that described for $[Ir(ppy)_2pi]Cl$ but using dmpip (0.063 g, 0.015 mmol) instead of dpip. Yield: 0.0725 g, 57.6%; elemental analysis calcd (%) for $C_{43}H_{33}N_7ClIr$: C 62.77, H 3.98, N 8.96; found: C 62.68, H 4.13, N 8.84; 1H NMR (500 MHz, $[D_6]DMSO$): δ = 9.29 (dd, J = 8.0, 1.5 Hz, 1H), 8.23 (ddd, J = 9.0, 6.0, 4.5 Hz, 3H), 8.12 (dd, J = 8.3, 5.1 Hz, 1H), 8.07 (d, J = 5.0 Hz, 1H), 7.94 (dd, J = 14.0, 7.5 Hz, 2H), 7.88 (dd, J = 14.5, 7.0 Hz, 2H), 7.81 (dd, J = 8.5, 5.0 Hz, 1H), 7.71–7.65 (m, 3H), 7.51–7.41 (m, 7H), 7.08–6.87 (m, 8H), 6.28 (dd, J = 12.0, 7.5 Hz, 2H), 3.03 ppm (s, 6H); ^{13}C NMR (125 MHz, $[D_6]DMSO$): δ = 167.32, 154.69, 151.49, 151.07, 150.65, 149.57, 148.60, 145.05, 144.69, 144.46, 139.20, 136.30, 132.83, 131.66, 130.75, 130.33, 130.23, 129.90, 129.66, 129.44, 128.99, 128.68, 128.13, 126.95, 126.56, 125.57, 124.37, 124.26, 122.84, 122.77, 120.47, 113.01 ppm; ES-MS (CH_3OH): m/z 916.30 $[M-Cl]^-$.

X-ray crystallography

X-ray diffraction measurements were performed using an Oxford-diffraction-Xcalibur-Nova diffractometer and a Rigaku R-Axis SPIDER image plate diffractometer with graphite-monochromated $Cu_{K\alpha}$ (λ = 1.54178 Å) and $Mo_{K\alpha}$ radiation (λ = 0.71073 Å), respectively. Absorption correction was applied using the SADABS program.^[42] The solution structures of **IrL2** and **IrL5** and full-matrix least-squares refinement based on F^2 were determined using the SHELXL-2014 program incorporated in the OLEX2 program package.^[43,44] All of the hydrogen atoms were included in the calculated positions and refined with isotropic thermal parameters riding on the positions of the parent atoms. The disordered chloroform and toluene molecules in **IrL5** were removed using the SQUEEZE routine in the PLATON software.^[45] CCDC 1059823 (**IrL2**) and 1059824 (**IrL5**) contain the supplementary crystallographic data for this paper. These data are provided free of charge by The Cambridge Crystallographic Data Centre.

Spectral analysis

For physiological applications, the photophysical and sensing properties of the **IrL1–IrL5** complexes were investigated in DMSO/PBS (10 μ M, pH 7.4, v/v, 1:999) buffer solutions. Both the absorption and emission spectra were recorded in standard 3.0 cm quartz

cells. The mixture was equilibrated for 5 min prior to the measurement. The excitation wavelength was 382 nm, and both slits were set to 10 nm for the emission spectra.

Determination of two-photon absorption cross-sections

The two-photon absorption spectra of probes determined over a broad spectral region by the typical two-photon induced fluorescence (TPF) method relative to rhodamine B in methanol as standard. The two-photon fluorescence data were acquired using OpoletteTM 355 II (pulse width ≤ 100 fs, 80 MHz repetition rate, tuning range 720–860 nm, Spectra Physics Inc., USA). Two-photon fluorescence measurements were performed in fluorometric quartz cuvettes with IrL1–IrL5 at 5×10^{-4} M in methanol at 298 K. The experimental fluorescence excitation and detection conditions were conducted with negligible reabsorption processes, which can affect TPA measurements. The quadratic dependence of two-photon induced fluorescence intensity on the excitation power was verified for an excitation wavelength of 750 nm. The two-photon absorption cross-section of the probes was calculated at each wavelength according to Equation (1) in which I is the integrated fluorescence intensity, A is the integrated absorbance intensity, and n is the refractive index of solvent. The subscript r indicates the reference sample, and s represents the test sample.

$$\varphi_s = \varphi_r \frac{I_s A_r n_s}{I_r A_s n_r} \quad (1)$$

Cell viability assay

HeLa cells were maintained as monolayer cultures in DMEM supplemented with 10% FBS and 1% antibiotic solution at 37 °C in a humidified atmosphere with 5% CO₂. The cytotoxicity of the iridium(III) complexes against HeLa cells was evaluated using the MTT assay. The exponentially grown HeLa cells were seeded in triplicate into 96-well plates at 1×10^4 cells per well. After incubation for 24 h, the cells were treated with IrL1–IrL5 at the concentration used for staining (200 nM) for various durations. To stain the viable cells, 12 μ L of MTT (5 mg mL⁻¹, Sigma) was added to each well. Then, the cells were incubated for another 4 h at 37 °C. The media was carefully removed to avoid disturbing the formazan crystals that had formed, and then 150 μ L of DMSO was added to dissolve the formazan crystals. The absorbance of the samples was measured at 595 nm using an ELISA reader (BioTek Instruments, Winooski, VT).

Confocal luminescence imaging

HeLa cells were incubated at a density of approximately 1×10^4 cells per mL in DMEM supplemented with 10% FBS as well as 1% penicillin and streptomycin (Gibco) at 37 °C in a humidified atmosphere with 5% CO₂. After incubation for 1 day, the cells were treated with 200 nM Ir^{III} complexes in DMEM for 15 min. After removing the DMEM and washing with PBS buffer three times to remove the remaining dye, the HeLa cells were further stained with MTG for 30 min. The cells were washed three times carefully with PBS buffer prior to luminescence imaging measurements. The cell images were captured with a monochromatic CoolSNAP FX camera (Roper Scientific, USA) and analyzed using the AxioVision 4.2 software (Carl Zeiss).

Three-dimensional multicellular spheroids were cultured using the liquid overlay method.^[32] HeLa cells in the exponential growth phase were dissociated by trypsin to obtain single-cell suspensions. Then, 4000 diluted HeLa cells were transferred to 1% agarose-

coated transparent 96-well plates with 200 μ L of DMEM containing 10% FBS (1% penicillin/streptomycin). The single cells generated 3D multicellular spheroids approximately 700 nm in diameter on the fourth day at 37 °C in a 5% CO₂ incubator with a humidified atmosphere. After formation, the spheroids were treated with 500 nM Ir^{III} complexes for 0.5 h to ensure that the complexes penetrated throughout the spheroids. The spheroids were then imaged using confocal laser scanning microscopy.

ICP-MS analysis

HeLa cells were plated at a density of approximately 3×10^5 cells per mL in 25 cm² culture plates (Corning) with 6 mL of DMEM with 10% FBS. IrL1–IrL5 (200 nM) was added to the culture medium and incubated for 5 min or for a time within the range of 0–30 min at 37 °C. After digestion with trypsin (Gibco), the HeLa cells were counted and divided into two samples. The first sample was subjected to nuclear isolation using a nucleus extraction kit. The second sample was subjected to mitochondrial extraction using a cytoplasm and mitochondria extraction kit (Shanghai Sangon Biological Engineering Technology & Services Co. Ltd.). The samples were digested in 65% HNO₃ at room temperature for at least one day. Each sample was diluted with double distilled water to obtain 2% HNO₃ sample solutions. The iridium concentration in the two samples was determined by inductively coupled plasma mass spectrometry (ICP-MS Thermo Elemental Co., Ltd.).

Flow cytometry analysis

HeLa cells at a density of 1×10^5 cells per mL were cultured in 6-well plates for 24 h in an incubator and then treated with IrL2 (200 nM) in DMEM supplemented with 10% FBS for 5 min at 37 °C. Then, the cells were trypsinized and washed with PBS three times. These cell uptake samples were analyzed with a FACSCanto II instrument (BD Biosciences).

Acknowledgements

This work was supported by the 973 program (Nos. 2015CB856301), the National Science Foundation of China (Nos. 21172273, 21171177, and 21471164), and the Program for Changjiang Scholars and Innovative Research Team in the University of China (No. IRT1298).

Keywords: cyclometalation • imaging agents • iridium • mitochondrial tracking • two-photon excitation

- [1] a) Y. L. P. Ow, D. R. Green, Z. Hao, T. W. Mak, *Nat. Rev. Mol. Cell Biol.* **2008**, *9*, 532–542; b) G. Kroemer, L. Galluzzi, C. Brenner, *Physiol. Rev.* **2007**, *87*, 99–163; c) B. Kornmann, E. Currie, S. R. Collins, M. Schuldiner, J. Nunari, J. S. Weissman, P. Walter, *Science* **2009**, *325*, 477–481.
- [2] a) Y. Chen, G. W. Dorn, *Science* **2013**, *340*, 471–475; b) B. C. Dickinson, C. J. Chang, *Nat. Chem. Biol.* **2011**, *7*, 504–511.
- [3] S. Gandre-Babbe, A. M. van der Blik, *Mol. Biol. Cell* **2008**, *19*, 2402–2412.
- [4] P. Mishra, D. C. Chan, *Nat. Rev. Mol. Cell Biol.* **2014**, *15*, 634–646.
- [5] Y. Yang, Q. Zhao, W. Feng, F. Li, *Chem. Rev.* **2013**, *113*, 192–270.
- [6] R. P. Haugland, *Handbook of Fluorescent Probes and Research Chemicals* (Ed.: M. T. Z. Spence), Molecular Probes, Eugene, **1996**.
- [7] H. Kobayashi, M. Ogawa, R. Alford, P. L. Choyke, Y. Urano, *Chem. Rev.* **2010**, *110*, 2620–2640.
- [8] G. P. Pfeifer, Y.-H. You, A. Besaratinia, *Mutat. Res. M.* **2005**, *571*, 19–31.
- [9] Y. Chen, L. Qiao, L. Ji, H. Chao, *Biomaterials* **2014**, *35*, 2–13.

- [10] Q. Zhao, C. Huang, F. Li, *Chem. Soc. Rev.* **2011**, *40*, 2508–2524.
- [11] a) Y. Chi, P. T. Chou, *Chem. Soc. Rev.* **2007**, *36*, 1421–1431; b) Y. You, *Curr. Opin. Chem. Biol.* **2013**, *17*, 699–707.
- [12] a) Y. Y. Zhou, J. L. Jia, W. F. Li, H. Fei, M. Zhou, *Chem. Commun.* **2013**, *49*, 3230–3232; b) G. L. Zhang, H. Y. Zhang, Y. Gao, R. Tao, L. J. Xin, J. Y. Yi, F. Y. Li, W. L. Liu, J. Qiao, *Organometallics* **2014**, *33*, 61–68; c) Q. Zhang, R. Cao, H. Fei, M. Zhou, *Dalton Trans.* **2014**, *43*, 16872–16879; d) C. L. Ho, K. L. Wong, H. K. Kong, Y. M. Ho, C. T. Chan, W. M. Kwok, K. S. Leung, H. L. Tam, M. H. Lam, X. F. Ren, A. M. Ren, J. K. Feng, W. Y. Wong, *Chem. Commun.* **2012**, *48*, 2525–2527; e) C. H. Leung, H. J. Zhong, H. Yang, Z. Cheng, D. S. H. Chan, V. P. Y. Ma, R. Abagyan, C. Y. Wong, D. L. Ma, *Angew. Chem. Int. Ed.* **2012**, *51*, 9010–9014; *Angew. Chem.* **2012**, *124*, 9144–9148; f) H. Z. He, K. H. Leung, W. Wang, D. S. Chan, C. H. Leung, D. L. Ma, *Chem. Commun.* **2014**, *50*, 5313–5315; g) K. H. Leung, H. Z. He, W. Wang, H. J. Zhong, D. S. H. Chan, C. H. Leung, D. L. Ma, *ACS Appl. Mater. Interfaces* **2013**, *5*, 12249–12253.
- [13] a) P. Autier, P. Boyle, *Nat. Clin. Pract. Oncol.* **2008**, *5*, 178–179; b) D. L. Ma, H. J. Zhong, W. C. Fu, D. S. H. Chan, H. Y. Kwan, W. F. Fong, L. H. Chung, C. Y. Wong, C. H. Leung, *PLoS One* **2013**, *8*, e60114; c) G. Li, Q. Lin, L. Ji, H. Chao, *J. Mater. Chem. B* **2014**, *2*, 7918–7926.
- [14] a) S. S. Zhou, X. Xue, J. F. Wang, Y. Dong, B. Jiang, D. Wei, M. L. Wan, Y. Jia, *J. Mater. Chem.* **2012**, *22*, 22774–22780; b) L. Li, J. Ge, H. Wu, Q. H. Xu, S. Q. Yao, *J. Am. Chem. Soc.* **2012**, *134*, 12157–12167; c) F. Helmchen, W. Denk, *Nat. Methods* **2005**, *2*, 932–940; d) M. Pawlicki, H. A. Collins, R. G. Denning, H. L. Anderson, *Angew. Chem. Int. Ed.* **2009**, *48*, 3244–3266; *Angew. Chem.* **2009**, *121*, 3292–3316; e) W. R. Zipfel, R. M. Williams, W. W. Webb, *Nat. Biotechnol.* **2003**, *21*, 1369–1377; f) H. M. Kim, B. R. Cho, *Acc. Chem. Res.* **2009**, *42*, 863–872.
- [15] a) F. Pampaloni, E. G. Reynaud, E. H. K. Stelzer, *Nat. Rev. Mol. Cell Biol.* **2007**, *8*, 839–845; b) R. I. Dmitriev, A. V. Zhdanov, Y. M. Nolan, D. B. Papkovsky, *Biomaterials* **2013**, *34*, 9307–9317.
- [16] a) Y. Chen, L. P. Qiao, B. L. Yu, G. Y. Li, C. Y. Liu, L. N. Ji, H. Chao, *Chem. Commun.* **2013**, *49*, 11095–11097; b) C. Jin, J. Liu, Y. Chen, G. Li, R. Guan, P. Zhang, L. Ji, H. Chao, *Dalton Trans.* **2015**, *44*, 7538–7547; c) Y. Chen, W. Xu, J. Zuo, L. Ji, H. Chao, *J. Mater. Chem. B* **2015**, *3*, 3306–3314; d) X. Chen, L. Sun, Y. Chen, X. Cheng, W. Wu, L. Ji, H. Chao, *Biomaterials* **2015**, *58*, 72–81; e) G. Li, Q. Lin, L. Sun, C. Feng, P. Zhang, B. Yu, Y. Chen, Y. Wen, H. Wang, L. Ji, H. Chao, *Biomaterials* **2015**, *53*, 285–295.
- [17] W. Xu, J. Zuo, L. Wang, L. Ji, H. Chao, *Chem. Commun.* **2014**, *50*, 2123–2125.
- [18] S. Serroni, A. Juris, S. Campagna, M. Venturi, G. Denti, V. Balzani, *J. Am. Chem. Soc.* **1994**, *116*, 9086–9091.
- [19] K. Nakamaru, *Bull. Chem. Soc. Jpn.* **1982**, *55*, 2697–2705.
- [20] a) S. M. Borisov, C. Larndorfer, I. Klimant, *Adv. Funct. Mater.* **2012**, *22*, 4360–4368; b) S. Prior, A. Kim, T. Yoshihara, S. Tobita, T. Takeuchi, M. Higuchi, *PLoS One* **2014**, *9*, e88911; c) P. Zhang, H. Huang, Y. Chen, J. Wang, L. Ji, H. Chao, *Biomaterials* **2015**, *53*, 522–531; d) I. Kitanovic, S. Can, H. Alborzinia, A. Kitanovic, V. Pierroz, A. Leonidova, A. Pinto, B. Spingler, S. Ferrari, R. Molteni, A. Steffen, N. Metzler-Nolte, S. Wölfl, G. Gasser, *Chem. Eur. J.* **2014**, *20*, 2496–2507.
- [21] Q. Zhao, M. X. Yu, L. X. Shi, S. J. Liu, C. Y. Li, M. Shi, Z. G. Zhou, C. H. Huang, F. Y. Li, *Organometallics* **2010**, *29*, 1085–1091.
- [22] D. Gerlier, N. Thomasset, *J. Immunol. Methods* **1986**, *94*, 57–63.
- [23] C. A. Puckett, J. K. Barton, *Biochemistry* **2008**, *47*, 11711–11716.
- [24] G. H. Cheng, J. L. Fan, W. Sun, K. Sui, X. Jin, J. Y. Wang, X. J. Peng, *Analyst* **2013**, *138*, 6091–6096.
- [25] Y. Li, C. P. Tan, W. Zhang, L. He, L. N. Ji, Z. W. Mao, *Biomaterials* **2015**, *39*, 95–104.
- [26] C. Li, M. Yu, Y. Sun, Y. Wu, C. Huang, F. Li, *J. Am. Chem. Soc.* **2011**, *133*, 11231–11239.
- [27] K. Y. Zhang, K. K. W. Lo, *Inorg. Chem.* **2009**, *48*, 6011–6025.
- [28] A. Sorkin, M. von Zastrow, *Nat. Rev. Mol. Cell Biol.* **2009**, *10*, 609–622.
- [29] S. E. A. Gratton, P. A. Ropp, P. D. Pohlhaus, J. C. Luft, V. J. Madden, M. E. Napier, J. M. DeSimone, *Proc. Natl. Acad. Sci. USA* **2008**, *105*, 11613–11618.
- [30] a) C. X. a. W. Webb, *J. Opt. Soc. Am. B* **1996**, *13*, 481–491; b) M. D. a. A. R. Nikolay, S. Makarov, *Opt. Express* **2008**, *16*, 4029–4047.
- [31] a) T. Furuta, S. S.-H. Wang, J. L. Dantzker, T. M. Dore, W. J. Bybee, E. M. Callaway, W. Denk, R. Y. Tsien, *Proc. Natl. Acad. Sci. USA* **1999**, *96*, 1193–1200; b) C. K. Koo, L. K. So, K. L. Wong, Y. M. Ho, Y. W. Lam, M. H. Lam, K. W. Cheah, C. C. Cheng, W. M. Kwok, *Chem. Eur. J.* **2010**, *16*, 3942–3950.
- [32] J. B. Kim, R. Stein, M. J. O'Hare, *Breast Cancer Res. Treat.* **2004**, *85*, 281–291.
- [33] D. Drasdo, S. Hohme, *Phys. Biol.* **2005**, *2*, 133–147.
- [34] C. W. Leung, Y. Hong, S. Chen, E. Zhao, J. W. Lam, B. Z. Tang, *J. Am. Chem. Soc.* **2013**, *135*, 62–65.
- [35] a) V. Fernández-Moreira, F. L. Thorp-Greenwood, M. P. Coogan, *Chem. Commun.* **2010**, *46*, 186–202; b) J. R. Casey, S. Grinstein, J. Orlowski, *Nat. Rev. Mol. Cell Biol.* **2010**, *11*, 50–61.
- [36] J. R. Friedman, J. Nunnari, *Nature* **2014**, *505*, 335–343.
- [37] Y. Reis, M. Bernardo-Faura, D. Richter, T. Wolf, B. Brors, A. Hamacher-Brady, R. Eils, N. R. Brady, *PLoS One* **2012**, *7*, e28694.
- [38] A. Harriman, L. J. Mallon, G. Ulrich, R. Ziessel, *ChemPhysChem* **2007**, *8*, 1207–1214.
- [39] a) M. Karbowski, R. J. Youle, *Cell Death Differ.* **2003**, *10*, 870–880; b) L. Scorrano, M. Ashiya, K. Buttler, S. Weiler, S. A. Oakes, C. A. Mannella, S. J. Korsmeyer, *Dev. Cell* **2002**, *2*, 55–67.
- [40] M. Yamada, Y. Tanaka, Y. Yoshimato, S. Kuroda, I. Shima, *Bull. Chem. Soc. Jpn.* **1992**, *65*, 1006–1011.
- [41] M. Nonoyama, *Bull. Chem. Soc. Jpn.* **1974**, *47*, 767–768.
- [42] R. H. Blessing, *Acta Crystallogr. Sect. A* **1995**, *51*, 33–38.
- [43] G. M. Sheldrick, *Acta Crystallogr. Sect. A* **2008**, *64*, 112–122.
- [44] O. V. Dolomanov, L. J. Bourhis, R. J. Gildea, J. A. K. Howard, H. Puschmann, *J. Appl. Crystallogr.* **2009**, *42*, 339–341.
- [45] A. L. Spek, *Acta Crystallogr. Sect. D* **2009**, *65*, 148–155.

Received: May 13, 2015

Published online on July 21, 2015